

FEDSM-ICNMM2010 - Windows Internet Explorer

E:\ASME-Montreal-CD\index.html

DAEMON Tools Lite AstroBurn Products News [0/0] Weather Radio player IP-lookup Convert Select

Favorites Suggested Sites Web Slice Gallery

FEDSM-ICNMM2010

Page Safety Tools

ASME 2010

3rd Joint US-European Fluids Engineering Summer Meeting and 8th International Conference on Nanochannels, Microchannels, and Minichannels

August 1 - 5, 2010 Montreal, Canada

Home About FEDSM-ICNMM2010 Author Index Search Select a track..

Technical Tracks

- 3rd Joint US-European Fluids Engineering Summer Meeting
- 8th International Conference on Nanochannels, Microchannels, and Minichannels
- 7th International Symposium on Fluid-Structure Interactions, Flow-Sound Interactions, and Flow-Induced Vibration & Noise

Welcome to the FEDSM-ICNMM2010 DVD.

This DVD contains the final papers of the ASME 2010 3rd Joint US-European Fluids Engineering Summer Meeting and 8th International Conference on Nanochannels, Microchannels, and Minichannels. To locate papers, you can do one of the following:


1. [Search](#). You can perform a fielded search of the title, author(s) name, affiliation or paper number.
2. Review the papers listed in the tracks.
3. Browse the [Author Index](#).

This DVD is best viewed with a Java 1.4.2 (or higher) enabled web browser.

You will need Acrobat Reader 7.0 or higher to view the PDF files.







Computer | Protected Mode: Off

EN 5:38 PM 8/23/2010

FEDSM-ICNMM2010 - Windows Internet Explorer

E:\ASME-Montreal-CD\index.html

DAEMON Tools Lite AstroBurn Products News [0/0] Weather Radio player IP-lookup Convert Select

Favorites Suggested Sites Web Slice Gallery

FEDSM-ICNMM2010

Home About FEDSM-ICNMM2010 Author Index Search Select a track..

ASME 2010
3rd Joint US-European Fluids Engineering Summer Meeting and
8th International Conference on Nanochannels, Microchannels, and Minichannels
August 1 - 5, 2010 Montreal, Canada

Khezziar, Lyes
Experimental Characterization of Air-Entrainment in a Plunging Water Jet System Using Particle Image Velocimetry (PIV) [FEDSM/ICNMM2010-30225]
Flow Instabilities and Heat Transfer in Buoyancy Driven Flows of Inelastic Non-Newtonian Fluids in Inclined Rectangular Cavities [FEDSM/ICNMM2010-30243]

Khodabandeh, R.
Two Phase Heat Transfer of Ammonia in a Mini/Micro Channel [FEDSM/ICNMM2010-30302]
Two Phase Pressure Drop of Ammonia in a Mini/Micro-Channel [FEDSM/ICNMM2010-31021]

Khosla, A.
Pressure Drop in Microchannels Filled With Porous Media [FEDSM/ICNMM2010-30559]

Kianifar, Ali
Blade Curve Influences on Performance of Savonius Rotors: Experimental and Numerical [FEDSM/ICNMM2010-30919]
Numerical Analysis of Thermal Conductivity of Non-Charring Material Ablation Carbon-Carbon and Graphite With Considering Chemical Reaction Effects, Mass Transfer and Surface Heat Transfer [FEDSM/ICNMM2010-31009]

Kil, Hyun Gwon
An Aero-Acoustic Performance Prediction Method of Sirocco Fan [FEDSM/ICNMM2010-31040]

Kim, Daeioona

Computer | Protected Mode: Off

5:39 PM
8/23/2010

ICNMM2010-30919

BLADE CURVE INFLUENCES ON PERFORMANCE OF SAVONIUS ROTORS: EXPERIMENTAL AND NUMERICAL

Ali Kianifar

Department of Mechanical
engineering
Ferdowsi University of Mashhad,
Mashhad, Khorasan, IRAN
Email: a_kianifar@yahoo.com

Morteza Anbarsooz

Department of Mechanical
engineering
Ferdowsi University of Mashhad,
Mashhad, Khorasan, IRAN
Email: m.anbarsooz@gmail.com

Mohammad Javadi

Department of Mechanical
engineering
Ferdowsi University of Mashhad,
Mashhad, Khorasan, IRAN
Email: mohammad.javadi@gmail.com

ABSTRACT

In this study, the effect of blade curve on the power coefficient of a Savonius rotor is investigated by means of numerical simulation and wind tunnel tests. The tests were conducted on six rotors with identical dimensions but different blade curves, and the influences of blade curve and Reynolds number were studied. Followed by a simulation of the flow field around rotors with identical semi-circular curves and different overlaps, torque was calculated using pressure distribution on the blade surface, and the effect of Reynolds number and blade curve were studied on torque as well. Results indicate that changing the blade curve affects the power coefficient and torque by causing different drag coefficients. Also the rotor that yields the highest power coefficient and torque in one revolution compared with other rotors is highlighted.

INTRODUCTION

The task of wind turbines is to convert the wind power into mechanical energy, as in windmills, or producing electricity. Wind turbines fall into two main categories: vertical-axis and horizontal-axis. Horizontal-axis turbines are generally economical only in places where the wind is permanent and has a high average speed [1]. These turbines have the characteristics of relatively low torque and high rotational speed and are mostly used to generate electricity. On the other hand, vertical-axis turbines are simple in construction and operate independently of the wind direction. Unlike the horizontal-axis turbines, these turbines have low rotational speed and high torque, and have typically been used for water pumping in agriculture and industry because of their low construction cost. In vertical-axis turbines, the axis of the rotor shaft is arranged vertically and perpendicular to the wind direction. As a result, after a half rotation, the area swept by the

wind is forced to move against the wind direction thus reducing the power coefficient. Therefore, blade curve is of great importance [1, 2]. A commonly employed vertical-axis turbine design is the Savonius rotor which has two semi-cylindrical blades with a semi-circular cross-section (fig. 1). Its principle of operation is based on the difference in drag between the convex and concave parts of the semi-circle (the principle of drag difference). The principal parameters that define the blade curve of a Savonius rotor are shown in figure 2.

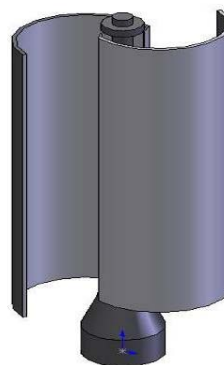


Figure 1. SAVONIUS ROTOR

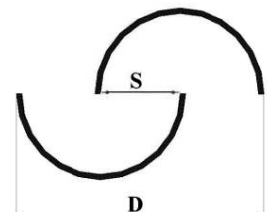


Figure 2. THE GEOMETRICAL
PARAMETERS OF SAVONIUS
BLADE CURVE

Numerous studies have been conducted on the blade curve of these rotors for the purpose of reducing drag coefficient while moving against the wind, and increasing it while moving in the wind direction. Savonius proposed a polynomial curve of order 4 which is as follows[3]:

$$y = -3.4868x^4 + 8.16507x^3 - 7.5605x^2 + 2.8507x + 0.040493$$

On the way to increase the efficiency of these rotors, Burçin Deda Altan [4, 5] used a curtain, designed to prevent the torque that occurs on the convex blade of the rotor in the negative direction, this curtain has been placed in front of the rotor. They investigated the effect of the existence of this curtain experimentally and numerically and showed that long curtain dimension will cause an increase in the static torque values. Kunio Irabu [6] investigated a method to prevent Savonius rotor from strong wind disaster under various wind power using a guide-box tunnel. The twisted blades in a three-bladed rotor system have been tested in a low speed wind tunnel, and its performance has been compared with conventional semicircular blades (with twist angle of 0) by U.K. Saha [7]. He [8] also conducted wind tunnel tests to assess the aerodynamic performance of single-, two- and three-stage Savonius rotor systems for both semicircular and twisted blades. In order to decrease the variation in coefficient of static torque which exists in conventional Savonius rotors, M.A. Kamojia [9] conducted performance tests on helical Savonius rotors with a twist of 90.

In present study, the effect of blade curve and the rotors principal parameters on the power coefficient of a Savonius rotor is investigated both numerically and experimentally. The power coefficient is calculated for different values of Reynolds number and different angles of blades in one complete revolution of rotor, and then they are compared.

EXPERIMENTAL DETAIL

Tests were carried out on Savonius rotors with six different blade curves in a wind tunnel with a section of $0.5 \times 0.5 \text{ m}^2$ and length of 5 m. The rotor blades are placed 2.4 m away from the inlet to ensure that the flow is uniform. A schematic of the wind tunnel is shown in figure 3. The cross-section of rotors is depicted in figure 4. In rotors I through V, each blade curve is a semi-circle with a diameter of 16 cm and their overlaps, S , are 0, 3.2, 3.8, 6.4 and 7.2 cm respectively. Overlap causes the drag force to vary from the back to the front region of blade at different angles. Rotor VI has a Savonius curve whose dimensions are similar to those of rotor IV. Rotor height, h , of all models is 30cm and blade thickness is 1mm.

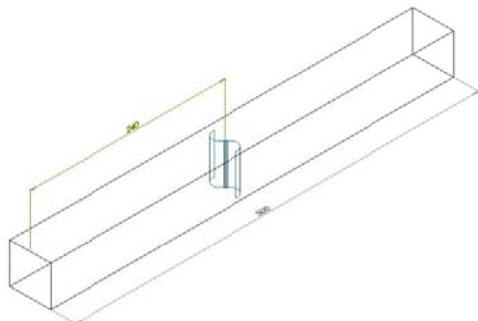


Figure 3. THE SCHEMATIC OF THE WIND TUNNEL (DIMENSIONS IN CM)

The power coefficient for each rotor was calculated from the measured rotor rotational speed and output torque, which were measured by the two dynamometers attached to the tip of each blade. All the tests were conducted under identical conditions with a wind speed ranging from 8 to 14 m/s. In the first step, rotational speed and torque of each rotor were measured in one revolution of the rotor and results for different rotors were compared. Then, the same test was carried out on each blade with different Reynolds numbers, different wind speeds, and the influence of Reynolds number on power coefficient was investigated. Results for rotors I and V are presented here. Using the previous test results, the average power coefficient in one revolution of rotor at a particular speed can be computed for each blade curve and be compared. With this comparison, optimum performance of the rotor can be determined.

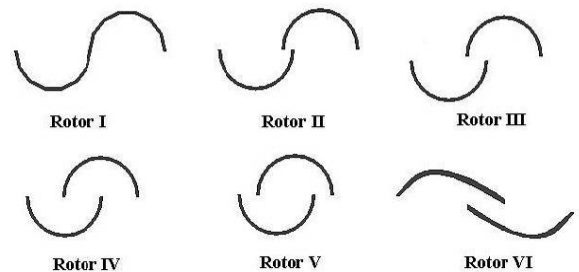


Figure 4. TEST ROTORS BLADE CURVE

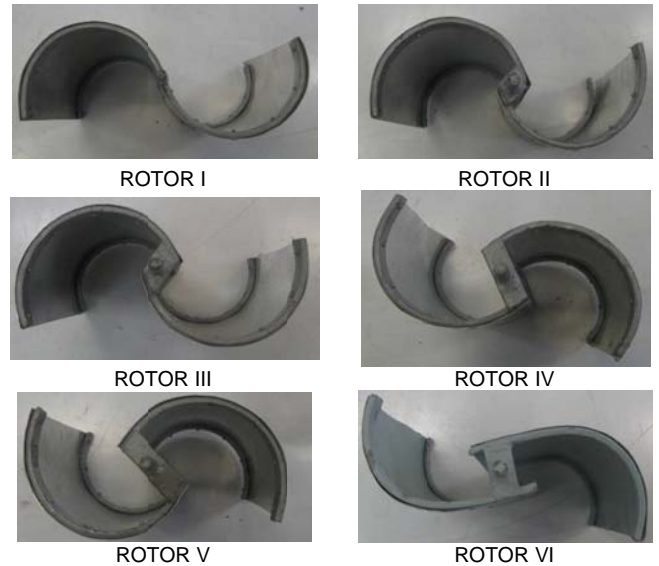


Figure 5. TEST ROTORS BLADES

Parameters like tip speed ratio; power coefficient and Reynolds number are defined as follows:

$$\text{Tip speed ratio} \quad \lambda = \frac{u}{V} = \frac{\omega D}{2V} \quad (1)$$

Power coefficient $C_p = \frac{2Fu}{\rho N^3 h D} \quad (2)$

Reynolds number $Re = \frac{VD}{\nu} \quad (3)$

Where V is wind velocity, D is rotor diameter, h is rotor height, u is tip speed and ω is rotor angular speed.

NUMERICAL METHOD

By simulating the wind flow through blades, torque and the effect of S/D , rotor overlap ratio, on the pressure exerted on the blades by wind are investigated. Hence, pressure distribution on blade surface is computed by solving the flow field, and torque is calculated by integrating pressure times the radial distance from the rotary axis. The principal equations in solving the flow field and computing pressure and velocity in different regions of rotor are continuity and momentum equations. Using a steady state, constant velocity coordinate system gives:

$$\frac{\partial}{\partial x_i}(\rho u_i) = 0 \quad (4)$$

$$\frac{\partial}{\partial x_i}(\rho u_i u_j) = -\frac{\partial p}{\partial x_i} + \frac{\partial \tau_{ij}}{\partial x_j} + \rho g_i + F_i \quad (5)$$

$$\tau_{ij} = \left[\mu \left(\frac{\partial u_i}{\partial x_j} + \frac{\partial u_j}{\partial x_i} \right) \right] - \frac{2}{3} \mu \frac{\partial u_i}{\partial x_i} \delta_{ij} \quad (6)$$

Where u_i and F_i are wind velocity and body forces respectively. In the study of rotor with variable angular velocity in a transient flow, the acceleration of the fluid should be augmented by additional terms that appear in the momentum equation:

$$\frac{\partial}{\partial t}(\rho v_r) + \nabla \cdot (\rho v_r v_r) + 2\Omega \times v_r + \Omega \times \Omega \times r + \rho \frac{\partial \Omega}{\partial t} \times r \quad (7)$$

To simplify the above equation, in numerical simulation of Savonius rotors, rotor angular velocity is considered to be constant [10, 11]. The governing equations are solved using the FluentTM 6.0 software.

GOVERNING EQUATIONS

In this study, $k - \varepsilon$ turbulence model has been employed to model Reynolds stress terms in momentum equations.

The turbulence kinetic energy and its rate of dissipation are obtained from the following transport equations [11]:

$$\rho \frac{Dk}{Dt} = \frac{\partial}{\partial x_i} \left[\left(\mu + \frac{\mu_t}{\sigma_k} \right) \frac{\partial k}{\partial x_i} \right] + G_k + G_b - \rho \varepsilon - Y_M \quad (8)$$

$$\rho \frac{D\varepsilon}{Dt} = \frac{\partial}{\partial x_i} \left[\left(\mu + \frac{\mu_t}{\sigma_\varepsilon} \right) \frac{\partial \varepsilon}{\partial x_i} \right] + C_{1\varepsilon} \frac{\varepsilon}{k} (G_k + C_{3\varepsilon} G_b) - C_{2\varepsilon} \rho \frac{\varepsilon^2}{k} \quad (9)$$

In these equations, G_k represents the generation of turbulence kinetic energy due to the mean velocity gradients and G_b is the generation of turbulence kinetic energy due to buoyancy, which is set equal to zero due to the absence of temperature gradients.

$$G_k = -\rho u_i' v_j' \frac{\partial u_j}{\partial x_i} \quad (10)$$

Y_M , which represents the contribution of the fluctuating dilatation in compressible flows with high Mach numbers, is also set equal to zero.

The governing equations in gaseous phase should be converted to algebraic equations to be solved numerically. To do so, in this paper, finite volume method has been used and the obtained equations were solved using simple algorithm [10]. Discretization of governing equations can be obtained by considering the unsteady conservation equation for transport of scalar quantity ϕ , written in integral form [12]:

$$\iint \rho \phi v \cdot dA = \iint \Gamma_\phi \nabla_\phi \cdot dA + \int S_\phi dV \quad (11)$$

Where V is control volume, v is velocity vector, and Γ_ϕ is diffusion coefficient for ϕ . This equation is applied to each control volume, or cell, in the computational domain. For a two-dimensional cell, the equation is written as follows:

$$\sum_f^{N_{faces}} v_f \phi_f A_f = \sum_f^{N_{faces}} \Gamma_\phi (\nabla_\phi)_n A_f + S_\phi V \quad (12)$$

Where v_f is mass flux through the face, ϕ_f is value of ϕ convected through face f , A_f is area of face f , and V is cell volume. Diffusion and convection flux values must be computed at the cell center (to represent a cell-average value). Here, this is accomplished using power-law scheme, which is more accurate than other methods [10]. In this method, the face value of variable ϕ is obtained using exact solution to the following one-dimensional convection-diffusion equation [12]:

$$\frac{\partial}{\partial x}(\rho u \phi) = \frac{\partial}{\partial x} \Gamma \frac{\partial \phi}{\partial x} \quad (13)$$

$$\frac{\phi(x) - \phi_0}{\phi_L - \phi_0} = \frac{\exp(Pe \frac{x}{L}) - 1}{\exp(Pe) - 1} \quad (14)$$

where Pe is the Peclet number. Now, the required discretized equations can be determined using simple algorithm and be solved by linear method which applies Gauss-Seidel

method in conjunction with three-diameter matrix algorithm [13].

RESULTS AND DISCUSSIONS

Figures 4 and 5 show the values of power coefficient of the test rotors as a function of tip speed ratio, at the Reynolds number of $Re = 1.5 \cdot 10^7$.

As shown in these figures, each rotor has an optimum performance at some certain tip speed ratios compared to other rotors. For example, rotors IV and V have larger values of power coefficient at small and large tip speed ratios in comparison with rotor I, whereas at average values, rotor I has a larger power coefficient.

To compare the rotors and determine the best curve, values of average or overall power coefficient can be used. Values of overall power coefficient are reported in figure 6. Note that rotor II has the best performance at different tip speed ratios. Rotors III and VI also have acceptable performances. Since the only difference among rotors I through V is their blade overlaps, comparison of power coefficients shows that increasing the overlap, S , from $S=0$ (rotor I) to $S=3.2\text{ cm}$ (rotor II) leads to a great increase in power coefficient and the forces resisting rotor motion decrease abruptly.

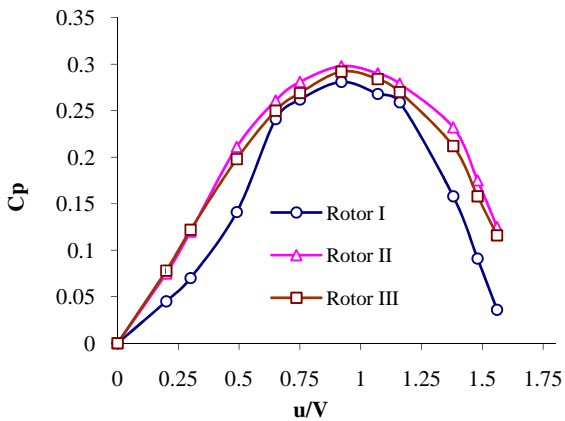


Figure 6. POWER COEFFICIENT OF ROTORS I TO III AS A FUNCTION OF TIP SPEED RATIO

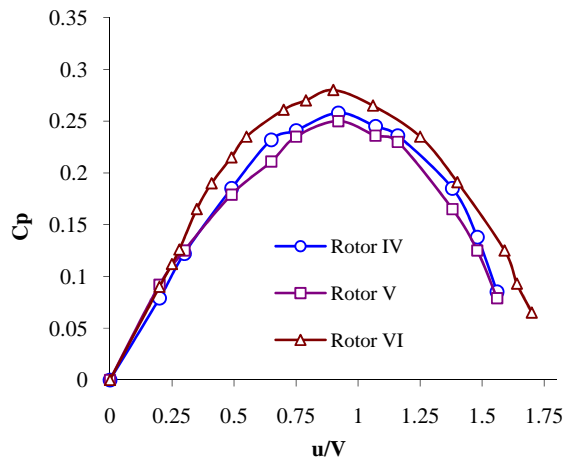


Figure 7. POWER COEFFICIENT OF ROTORS IV TO VI AS A FUNCTION OF TIP SPEED RATIO

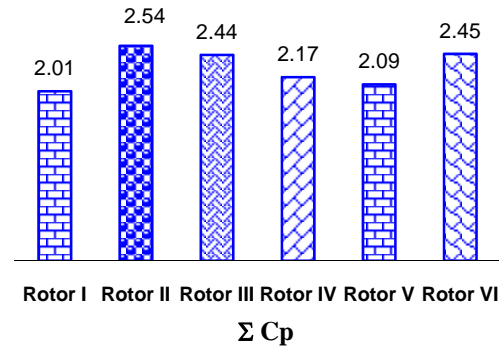
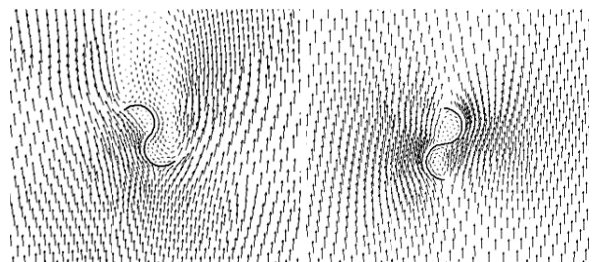


Figure 8. OVERALL POWER COEFFICIENT OF DIFFERENT ROTORS (I-VI)

On the other hand, increasing S from 3.2cm (rotor III) to 7.2cm (rotor V) reduces power coefficient. It can be concluded that the optimum range for S is from 0 to 3.2 cm. Influence of S on power coefficient can be investigated by determining velocity vectors around rotor blades which are obtained from numerical simulation [10, 11].



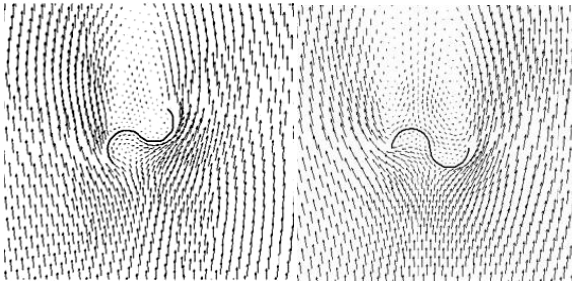


Figure 9. VELOCITY VECTORS AROUND ROTOR I

Figures 7 and 8 give a representation of velocity vectors obtained by numerical simulation of the flow field around rotors I and V at different rotor angles, which agree with previous studies [14]. Figures 9 and 10 show power coefficient of rotors I and IV at different Reynolds numbers. Note that increasing Reynolds number, that is wind speed, increases power coefficient. The maximum value of power coefficient appears at the range of $\lambda=0.8$ to $\lambda=1$ (tip peripheral speeds close to wind speed), which agree with previous studies (Hayashi et al. 2005). Average power coefficients of rotors I, II and IV are shown in figure 11. It can be noted that average power coefficient increases with increasing Reynolds number, but its rate decreases due to turbulence around the blades.

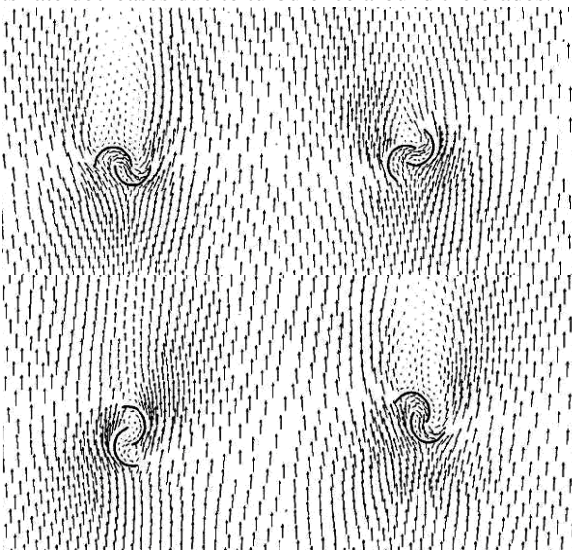


Figure 10. VELOCITY VECTORS AROUND ROTOR V

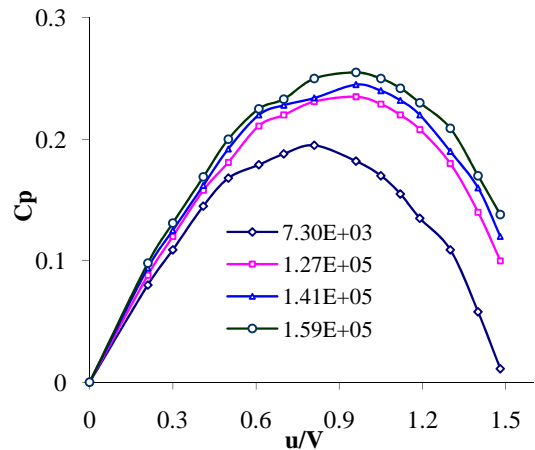


Figure 11. POWER COEFFICIENT OF ROTOR IV AT DIFFERENT REYNOLDS NUMBERS

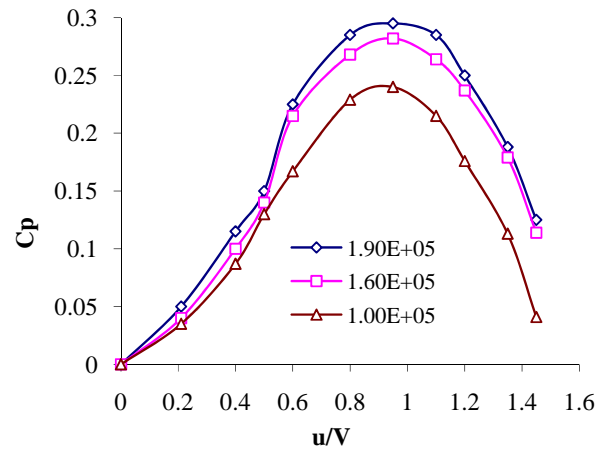


Figure 12. POWER COEFFICIENT OF ROTOR I AT DIFFERENT REYNOLDS NUMBERS

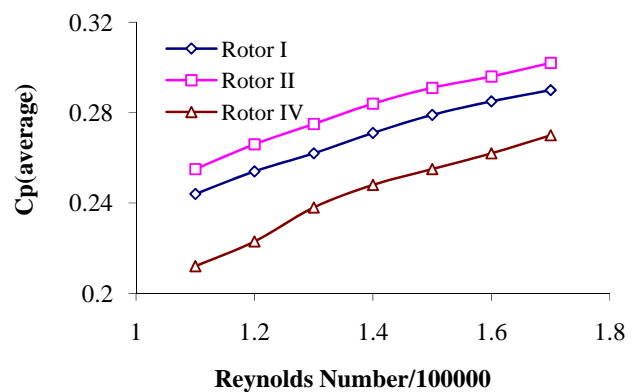


Figure 13. AVERAGE POWER COEFFICIENTS OF ROTORS I, II AND IV AT DIFFERENT REYNOLDS NUMBERS

Figures 12 to 15 show torque variations as a function of rotor angular position at different wind speeds, obtained by

numerical simulation. It can be noticed that torque increases with increasing wind speed and its maximum values appear near the angle of 60° and its minimum values appear near the angle of 120° for all test rotors. For rotor I, maximum values of torque occur at a wide range of angles, whereas the corresponding range is very small for other rotors.

Figure 16 shows torque variations as a function of angular position at wind speed of 12 m/s. At angles of 0° to 60° , rotor I has the highest values of torque, but its torque decreases drastically at angles larger than $\alpha = 60^\circ$ and this decrease continues up to $\alpha = 160^\circ$. It can be noted that rotor II has the largest output torque on a whole revolution of the rotor. Figure 17 indicates that output torque is a function of square root of wind speed, and power coefficient is a function of wind speed with a power of 3, which conforms to the numerical simulation results. Since this correlation applies to all rotors, in here, the result is only presented for rotor I.

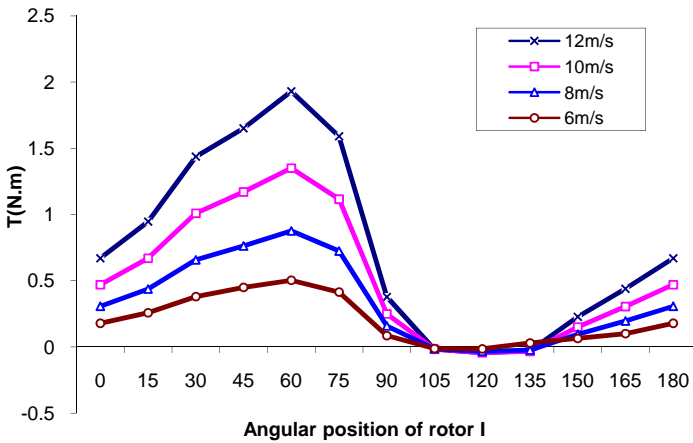


Figure 14. TORQUE OF ROTOR I AS A FUNCTION OF ANGULAR POSITION AT DIFFERENT REYNOLDS NUMBERS

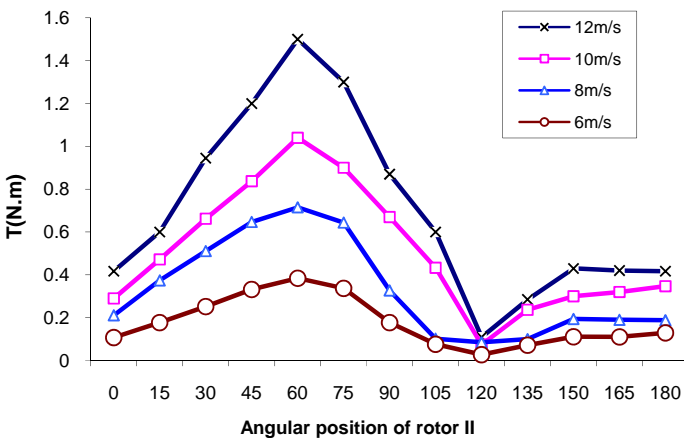


Figure 15. TORQUE OF ROTOR II AS A FUNCTION OF ANGULAR POSITION AT DIFFERENT REYNOLDS NUMBERS

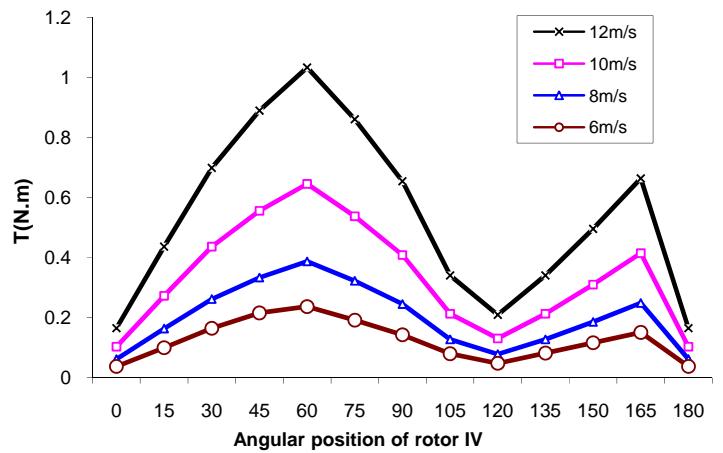


Figure 16. TORQUE OF ROTOR IV AS A FUNCTION OF ANGULAR POSITION AT DIFFERENT REYNOLDS NUMBERS

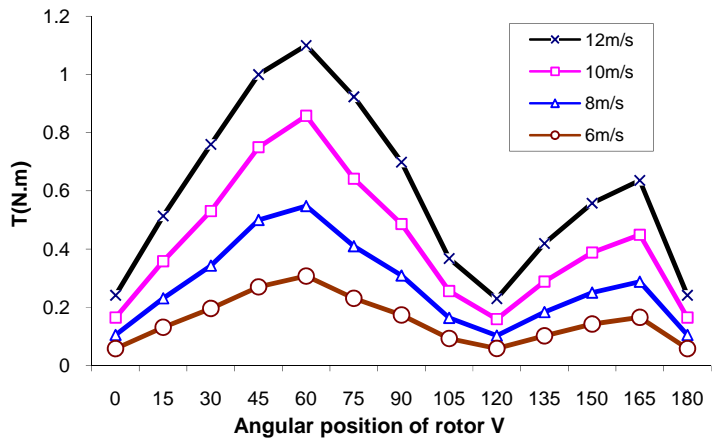


Figure 17. TORQUE OF ROTOR V AS A FUNCTION OF ANGULAR POSITION AT DIFFERENT REYNOLDS NUMBERS

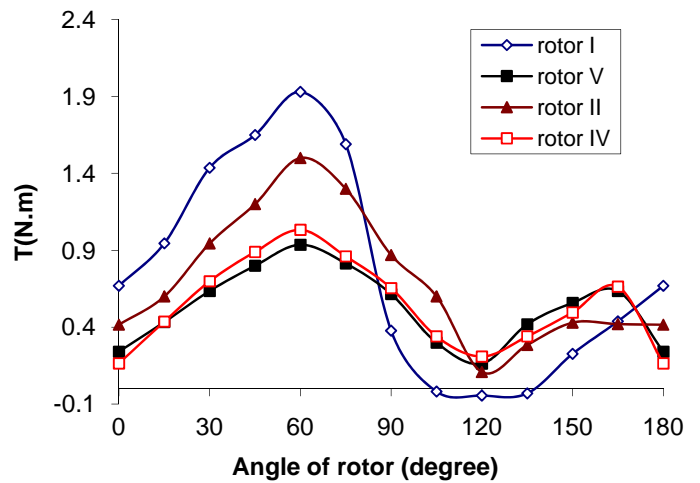


Figure 18. OUTPUT TORQUE OF TEST ROTORS AS A FUNCTION OF ANGULAR POSITION AT A WIND SPEED OF 12M/S

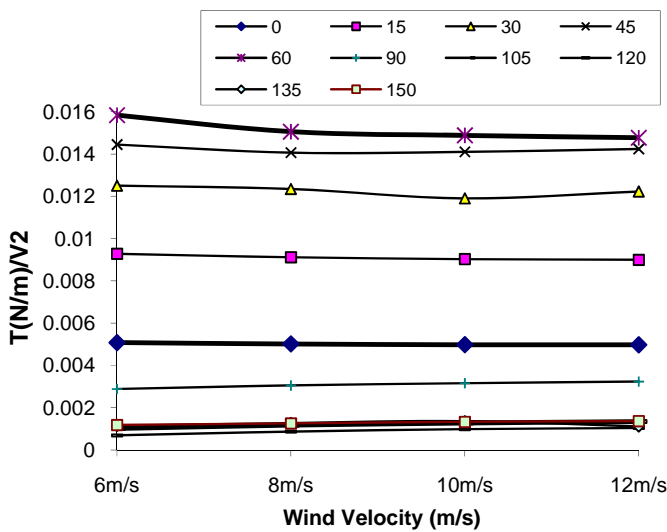


Figure 19. RATIO OF TORQUE TO ROTOR SPEED RATIO AS A FUNCTION OF WIND SPEED

CONCLUSION

In this study, wind tunnel tests were conducted on six rotors with different blade curves and the flow field around rotors was simulated numerically. Results, obtained by experimental and numerical analysis, can be summarized as follows:

- Rotors II through V have higher power coefficients due to their overlaps. On the other hand, increasing the overlap to a great extent decreases power coefficient. In this study, the optimum value was obtained to be $\frac{S}{D} = 0.2$.
- Increasing the overlap, S , from $S=0$ (rotor I) to $S=3.2$ cm (rotor II) leads to a great increase in power coefficient and the forces resisting rotor motion decrease abruptly. On the other hand, increasing S from 3.2cm (rotor III) to 7.2cm (rotor V) reduces power coefficient. It can be concluded that the optimum range for S is from 0 to 3.2 cm.
- Rotor II has the best blade curve.
- By increasing wind speed, which corresponds to higher Reynolds number, power coefficient increases greatly.
- The maximum value of power coefficient appears at the range of $\lambda = 0.8$ to $\lambda = 1$ (tip peripheral speeds close to wind speed)
- Average power coefficient increases with increasing Reynolds number, but its rate decreases due to turbulence around the blades.
- Torque increases with increasing wind speed and its

maximum values appear near the angle of 60° and its minimum values appear near the angle of 120° for all test rotors.

- At angles of 0° to 60° , rotor I has the highest values of torque, but its torque decreases drastically at angles larger than $\alpha = 60^\circ$ and this decrease continues up to $\alpha = 160^\circ$.
- Rotor II has the highest output torque on a whole revolution of the rotor.

REFERENCES

- [1] Manzoor, H. M., Nawazish, S. M. and Ram, P. R., 2008. "CFD Analysis of Low Speed Vertical Axis Wind Turbine with Twisted Blades" *Int. J Applied Engineering Research*, vol 3(1), pp. 149-159.
- [2] Moharrampour, J. 2001. "Optimization of wind energy and its applications in construction of Savonius rotors", MS thesis, Ferdowsi university of Mashhad, Mashhad, Iran.
- [3] Le Gourieres, D. 1982. *Wind Power Plants: Theory and Design*. Pergamon Press Ltd, England.
- [4] Burçin Deda Altan, Mehmet Atılğan, 2009. "The use of a curtain design to increase the performance level of a Savonius wind rotors", *Renewable Energy*, vol. 35, pp. 821-829.
- [5] Burçin Deda Altan, Mehmet Atılğan and Aydoğan zdamar, 2008. "An experimental study on improvement of a Savonius rotor performance with curtaining", *Experimental Thermal and Fluid Science*, vol. 32, pp. 1673-1678.
- [6] Irabu K., Nath Roy J., 2007. "Characteristics of wind power on Savonius rotor using a guide-box tunnel", *Experimental Thermal and Fluid Science*, vol. 32, pp. 580-586.
- [7] Saha U.K., Jaya Rajkumar M., 2006. "On the performance analysis of Savonius rotor with twisted blades", *Renewable Energy*, vol. 31, pp. 1776-1788.
- [8] Saha U.K., Thotla S. and Maity D., 2008. "Optimum design configuration of Savonius rotor through wind tunnel experiments", *J. Wind Engineering and Industrial Aerodynamics*, vol. 96, pp. 1359-1375.
- [9] Kamoji M.A., Kedare S.B. and Prabhu S.V., 2009. "Performance tests on helical Savonius rotors", *Renewable Energy*, vol. 34, pp. 521-529.
- [10] Cochran, B.C., Banks, D. and Taylor, S.J., 2004. "A three-tiered approach for designing and evaluating performance characteristics of novel WECS." *23rd ASME Wind Engineering Symposium*, Reno, Nevada, AIAA: 1362.
- [11] Kawamura, T., Hayashi, T., and Miyasha, K., 1998. "Application of the domain decomposition method to flow around the Savonius rotor", 12th International Conference on Domain Decomposition Methods.
- [12] Kozłowski, J.A. 1997. "Savonius rotor construction vertical axis wind machines from oil drums", VITA, Inc., USA.
- [13] Patankar, S. V. 1980. "Numerical heat transfer and fluid flow", John Benjamins publishing.

- [14] Menet, J. and Bourabaa, N. 2004. "Increase in the Savonius rotors efficiency via a parametric investigation", *European Wind Energy conference & exhibition*, London, UK.
- [15] Hayashi, T., Li, Y., Hara, Y. and Suzuki, K. 2005. "Wind tunnel tests on a three-stage out-phase Savonius rotor", *JSME International Journal*, vol. 48(1), pp. 9-16.